PRESERVATION OF CLAY MINERALS IN THE PRECAMBRIAN (1.1 GA) NONESUCH FORMATION IN THE VICINITY OF THE WHITE PINE COPPER MINE, MICHIGAN[1]

GEJING LI, JEFFREY L. MAUK,[2] AND DONALD R. PEACOR

Department of Geological Sciences, University of Michigan, Ann Arbor, Michigan 48109-1063

Abstract—The Middle Proterozoic (1.1 Ga) Nonesuch Formation, host of the stratiform copper deposit at White Pine, Michigan, consists of 200 m of principally dark grey clastic sediments which contain detritus obtained dominantly from underlying mafic to intermediate volcanic rocks. Clay minerals from samples collected from the mine area and drill holes up to 100 km away have been studied using SEM, EMPA, TEM and AEM. Two morphologies of phyllosilicates, both including white mica and chlorite, occur in the 'lower' Nonesuch Formation: (1) detrital-shaped and (2) matrix. Detrital-shaped phyllosilicate grains are up to 450 microns long with long axes parallel to bedding. Matrix phyllosilicates occur as packets typically <200 Å thick and as pore-filling cement.

TEM images of detrital-shaped chlorite generally display 14-Å periodicity, although 24-Å corrensite-like units occur locally. Most detrital-shaped chlorite from the mine area samples have a relatively restricted range of Fe/(Mg+Fe) ratios from 0.52 to 0.58, but the Fe/(Fe+Mg) ratios of detrital-shaped chlorite outside the mine area range from 0.27 to 0.64. TiO_2 crystals occur within and surrounding the detrital-shaped chlorite. Matrix chlorite has Fe/(Fe+Mg) ratios of 0.47 to 0.63, indicating that it is relatively homogeneous and enriched in Fe compared to detrital-shaped chlorite.

Detrital-shaped white mica occurs as a $2M_1$ polytype and generally has a phengitic composition. Matrix illite-rich I/S occurs as a $1M_d$ polytype, is K and Al deficient relative to end-member muscovite and contains significant Fe and Mg.

The data are consistent with homogenization of detrital-shaped chlorite in the White Pine mine area by hydrothermal fluids during copper mineralization. The TiO_2 crystals and corrensite-like units in detrital-shaped chlorite imply that it is at least in part derived from alteration of biotite. The presence of immature $1M_d$ illite-rich I/S and a one layer chlorite polytype with stacking disorder suggests that the matrix clays are in their original, post-smectite state of formation as consistent with an authigenic origin during early burial diagenesis; i.e., they have not undergone subsequent transformation even though sedimentation and ore deposition occurred prior to 1 Ga.

Key Words—Chlorite, Diagenesis, Illite, Mixed-layer illite/smectite, Nonesuch Formation, White mica.

INTRODUCTION

The wall rocks of hydrothermal ore deposits commonly display a pronounced alteration halo as a result of the interaction of ore-forming fluids with the surrounding country rocks. In many types of deposits, classic studies have led to zoning models that have provided powerful tools for mineral exploration. However, the more pronounced alteration halos are commonly associated with high-temperature ore formation, so that in "cooler" hydrothermal systems, the alteration halos tend to be less well-developed.

The White Pine sediment-hosted stratiform copper deposit is located in the Lake Superior portion of the 1.1 Ga-old Midcontinent rift system (Figure 1). With current reserves of approximately 170 million metric ton of ore grading 1.1 wt. % Cu, this is the largest and most intensively studied ore body of its class in North America. Other workers have documented a well-defined sulfide zonation which cross-cuts stratigraphy of the host Nonesuch Formation both in the mine area and on a regional scale (e.g., White and Wright 1966, Brown 1971, Figure 2). Mass balance calculations suggest that if the mineralizing fluids that formed the White Pine deposit contained 50 ppm copper, then water-rock ratios in sediments containing 1.1 wt. % copper would be 220/1 (e.g., White 1971). Indeed, many of the ore-bearing horizons in the mine area contain an average of 2–3 wt. % copper, and samples with copper contents of 8–10 wt. % are not uncommon, indicating that much higher water-rock ratios occurred locally. However, in spite of these high water-rock ratios, former studies have not documented any zoning in the silicate minerals in the rocks within and adjacent to the White Pine ore body.

The ground work for this study was laid by Sliney (1988), who examined both mineralized and unmineralized samples of the 'UZV' siltstone (in the 'upper shale,' see Figure 2) in the mine area with scanning electron microscopy (SEM) and electron microprobe analysis (EMPA). Several of her observations are par-
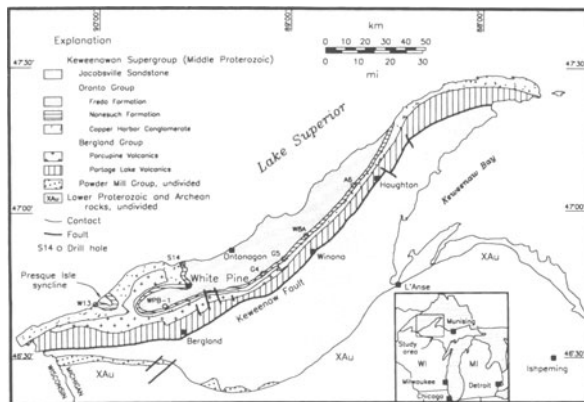
Figure 1. Location of the area studied on the Keweenawan Peninsula, northern Michigan.
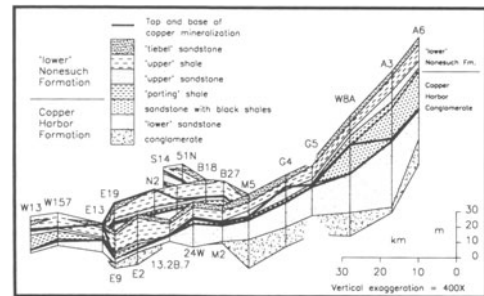

Figure 2. Generalized stratigraphy of the 'lower' Nonesuch Formation from Houghton, Michigan to the Presque Isle syncline. The White Pine mine is located in the vicinity of drill holes B18, N2 and 24W.

ticularly noteworthy: (1) Chlorite, which is the dominant phyllosilicate in the Nonesuch Formation, commonly occurs as detrital-shaped grains. These grains locally bend around other clastic grains, indicating that they were present during compaction of the sediments. (2) Some of these detrital-shaped chlorite grains contain interstratified stacks of white mica. (3) Chalcocite, which is the dominant ore mineral in the mine, commonly occurs within detrital-shaped chlorite grains, but it occurs only within chlorite packets; nowhere does chalcocite occur within the interstratified white mica. Outside the mineralized horizon, pyrite has the same textural relations: it is found only in chlorite layers, not in white mica layers of large detrital-shaped chlorite grains. (4) Within the area studied by Sliney (1988), the chemical composition of the detrital-shaped chlorite is relatively homogeneous both in mineralized and unmineralized strata. Collectively, these observations suggested that detrital-shaped chlorite was an authigenic phase, with a relatively homogeneous chemical composition, that had pseudomorphed one or more precursor detrital phases.

A lingering question remained after Sliney's (1988) investigation. Was the observed homogenization of the detrital-shaped chlorite in the vicinity of the White Pine mine a reflection of a larger zoning pattern? Because copper mineralization occurs in the 'lower' Nonesuch Formation for many tens of kilometers to the east and west of the mine area (Figure 2), the idea of a large hydrothermal alteration zone was compatible with the observed data.

This study had two principal objectives: (1) To test the hypothesis that the White Pine hydrothermal system has an alteration halo that is characterized, at least in part, by chemically homogeneous chlorite, and (2) to complete a detailed transmission electron microscopy (TEM) and analytical electron microscopy (AEM) study of the clay minerals in both mineralized and unmineralized samples of the 'lower' Nonesuch For-

mation in the Lake Superior portion of the Midcontinent rift system. Previous XRD data (e.g., Price and McDowell 1993) had indicated the presence of a smectite component (20–30%) to the illite, a surprising feature in samples of such great age, and one having significance with respect to the rate of transformation of smectite to illite.

GEOLOGICAL SETTING AND UNITS ANALYZED

The Keweenawan Supergroup (1.1 Ga) in the Lake Superior Basin (Figure 1) consists of a thick sequence of volcanic and sedimentary rocks which filled a portion of the Midcontinent rift system during Proterozoic time (White 1966, Chase and Gilmer, 1973, Daniels 1982, Cannon *et al* 1989). The stratigraphic section near White Pine consists of a basal unit of 5–13 km of mafic to intermediate flows of the Portage Lake Volcanics and the Porcupine Volcanics (Cannon and Nicholson 1992). The Porcupine Volcanics are overlain by the Copper Harbor Conglomerate, a thick wedge (up to 2 km) of coarse continental clastics which grade upward into the green to gray pyritic siltstones and shales (40–300 m) of the Nonesuch Formation (Figure 2). Overlying the Nonesuch Formation is up to 4 km of the dominantly red Freda Sandstone. The Copper Harbor Conglomerate, Nonesuch Formation, and Freda Sandstone form the Oronto Group and are believed to represent first-cycle sediments derived dominantly from the underlying volcanic rocks (Thwaites 1912, Daniels 1982, Elmore *et al* 1989).

Most workers that have attempted to constrain the P-T history of the White Pine region have utilized a variety of methods, and inferred that paleotemperatures remained less than 100°C during diagenesis and mineralization (e.g., Meinschein *et al* 1964, Brown 1971, White 1971, Nishioka 1983, Arehart 1992). However, based on illite smectite geothermometry, Price and McDowell (1993) concluded that maximum paleotemperatures may have ranged from 115°C in the Presque Isle Syncline, to 160°C in the White Pine re-

Table 1. Methods of study for samples analyzed.

Samples	Stratigraphic unit	Location	Comments	Analytical methods
420	'upper' Nonesuch Formation	[1]WPB-1	unmineralized	TEM & AEM
111	'UZV' (LNF)[2]	mine	mineralized	microprobe
139	'thinly' (LNF)	mine	mineralized	TEM & AEM
449	'thinly' (LNF)	DDH[3] G4	unmineralized	microprobe
511	'thinly' (LNF)	DDH A6	unmineralized	TEM & AEM
455	'DGM' (LNF)	DDH W8A	unmineralized	microprobe
421	'domino' (LNF)	mine	mineralized	TEM & AEM
453	'domino' (LNF)	DDH G5	mineralized	microprobe
517	'domino' (LNF)	DDH A6	unmineralized	TEM & AEM

[1] See also Figure 1 in Price and McDowell (1993).
[2] LNF: lower Nonesuch Formation.
[3] DDH: diamond drill hole.

gion, to 190°C near Houghton; on the other hand, Essene and Peacor (1995) emphasized the inherent inaccuracy of clay geothermometers. The collective data are thus consistent with an approximate maximum temperature of 100°C. Maximum burial of the Nonesuch Formation in the White Pine region has been bracketed between 1.5 and 3.6 km (e.g., Brown 1971, White 1971, Nishioka 1983).

Only the basal 1–4 m of the Nonesuch Formation within the White Pine mine contain economic concentrations of Cu minerals. The 'lower' Nonesuch Formation consists of alternating red and grey strata; red beds contain <1 wt. % Cu, whereas grey to black beds contain 2–4 wt. % Cu in the mine area. The 'domino' shale (in the 'parting' shale) and 'thinly' shale (in the 'upper' shale) are the two units studied in this investigation (Figure 2), as representative of other black shales in the region. Two fresh samples were collected from each of the two shales, one from the mine area and one from a drill hole (A6) 100 km northeast of the mine for TEM study. Samples 421 and 517 were collected from mineralized and unmineralized portions of the 'domino' shale respectively, and samples 139 and 511 were collected from mineralized and unmineralized portions of the 'thinly' shale, respectively. Following the precedent of White and Wright (1966), we classify "unmineralized" samples as those with <0.2 wt. % Cu, and "mineralized" samples as those with assays ≥0.2 wt. % Cu. In order to constrain the variations in clay minerals, a sample (420) was also collected from the 'upper' Nonesuch Formation from an area about 20 km southwest of the mine for comparison. In addition, some other drill hole samples were also studied by EMPA. A combination of Figure 2 and Table 1 gives the sample locations and analytical methods. Additional information about other drill hole samples was given by Mauk (1993).

Price and McDowell (1993) systematically studied clay fractions of sediments in the Nonesuch Formation and the overlying Freda Sandstone by XRD. Their data show that I/S expandability within the Nonesuch Formation is typically 10% or less. The only exception

occurs in drill hole WPB-1 where sample 420 was collected from the Nonesuch Formation, for which expandabilities vary from 25 to 30%. The expandable component in the Nonesuch Formation decreases away from WPB-1 to less than 5% at White Pine (only 20 km away).

METHODS

XRD data were obtained for the powdered bulk rock samples, using a Philips automated diffractometer with graphite monochromator and CuKα radiation (35 kV and 15 mA) and quartz as an internal standard to define the principal minerals. Chamosite (Fe-rich chlorite), phengitic muscovite and illite, quartz, albite, epidote, and pyrite were detected in all samples.

Polished thin sections were prepared with the surface approximately normal to bedding so that the optimum orientation could be obtained for scanning electron microscope (SEM) observations of textural relations, and so that the (001) planes of phyllosilicates would be preferentially oriented parallel to the electron beam for TEM observations. Following optical and SEM observation using back-scattered electron (BSE) imaging and X-ray energy dispersive spectral (EDS) analysis with a Hitachi S-570 scanning electron microscope operated at 15 kV to outline the areas of interest, ion-milled TEM specimens were prepared following the method described by Li et al (1994). In order to check the expandability of I/S in the sample matrix, sample 420, which was inferred to have the largest proportion of smectite, was chosen to be permanently expanded by L. R. White resin (Kim et al 1995) prior to TEM sample preparation. TEM observations and AEM analyses were obtained using a Philips CM12 scanning transmission electron microscope (STEM) fitted with a Kevex Quantum solid-state detector and computer system. The STEM was operated at an accelerating voltage of 120 kV and a beam current of ~10 μA to obtain TEM images and selected area electron diffraction (SAED) patterns. EDS data were obtained in scanning mode by rastering the beam over thin edges (100 × 2000 Å areas). Stationary point beam analysis was

also used in some areas so that grains as small as 100 Å in diameter could be analyzed. AEM quantitative chemical analyses were obtained by processing and calculating the EDS data in the thin-foil approximation (Cliff and Lorimer 1975), using experimentally determined k-ratios from the standards muscovite (K, Al), clinochlore (Mg, Al, Fe), albite (Na, Al), fayalite (Fe), rhodonite (Mn, Fe, Ca) and sphene (Ti, Ca). Chemical compositions of the coarse-grained detrital-shaped chlorite were also determined using a Cameca CA-MEBAX electron microprobe operated at 12 kV accelerating voltage and 10 nA beam current, and Gotthard adularia (K), Tiburon albite (Na), fluortopaz (F), geikielite (Ti), andalusite (Al), Marjalahti olivine (Mg), synthetic ferrosilite (Fe), Broken Hill rhodonite (Mn), diopside (Ca, Si), sanbornite (Ba), uvarovite (Cr) and Ba-Cl apatite (Cl) as standards. The ZAF corrections were carried out with Cameca programs.

RESULTS

SEM observations

Back-scattered electron (BSE) images (e.g., Figure 3) of both mineralized and unmineralized samples of the "thinly" and "domino" shales show that grains with subangular to subrounded shapes typical of detrital grains are surrounded by a matrix of finely crystallized chlorite and illite. Grains consist of subangular and irregular quartz, plagioclase (An $_{5-45}$), K-feldspar, chlorite, white mica, and epidote up to 50 μm in diameter with shapes typical of a detrital origin, and lithic fragments which primarily include mafic volcanic and subordinate silicic and intermediate volcanic fragments (c.f. Hite 1968). Other accessory minerals observed by SEM include sphene, rutile, apatite and zircon. Elongated chlorite and white mica grains show a preferred orientation subparallel to bedding (Figure 3). Such chlorite is referred to as "detrital-shaped chlorite" as it is shown below that it was originally detrital biotite. Chlorite makes up about 30% of the samples and occurs as tabular grains up to 450 μm long and 30 μm thick. The laths display varying degrees of deformation and locally bend around other clastic grains (Figure 3d), indicating that this type of chlorite was present before full compaction. Some chlorite laths contain subordinate intergrowths of white mica packets and could thus be referred to as "stacks." Within the unmineralized shale, the chlorite laths locally contain abundant equant to elongate inclusions of pyrite (e.g., Figure 3b). Similarly, chlorite laths in the mineralized shale commonly contain abundant inclusions of chalcocite. Qualitative EDS analysis demonstrates that chlorite generally is slightly Fe-rich relative to Mg. However, subordinate Mg-rich chlorite was also observed in association with Fe-rich chlorite in unmineralized shales, as indicated in part by its different contrast in BSE images (Figure 3b).

White mica constitutes approximately 8% of the shales and occurs as well-preserved tabular grains ranging up to 150 × 20 μm in size. It generally has a phengitic composition as determined by qualitative EDS analysis, but some white mica in unmineralized shales is near ideal muscovite in composition. In contrast to chlorite, no sulfide inclusions were observed in white mica. This relation also applies to the intergrowths of chlorite and white mica, and where white micas are observable, the sulfide inclusions never occur within the white mica packets; they are confined to the chlorite layers. Such relations were also observed in the 'UZV' siltstone in the Nonesuch Formation by Sliney (1988).

The dominant mineral in the very fine-grained matrix is chlorite; illite (or I/S) is much less abundant. The chlorite and illite (or I/S) matrix pervasively surrounds the large detrital-shaped clasts and fills embayments in the corroded silicate grains, indicating that it is an authigenic cement rather than a detrital component. Pyrite also commonly occurs in the matrix, both as single euhedral grains, and as clusters of euhedra. In mineralized shale, chalcocite commonly forms irregular interstitial grains in the matrix (Figure 3a).

TEM and AEM observations

Textural relationships. TEM images show that grains of detrital-shaped chlorite and white mica are generally oriented parallel to sedimentary bedding, and are characterized by much larger packet sizes than matrix phyllosilicates. The matrix phyllosilicates commonly have (001) oriented parallel to the boundaries of detrital-shaped material where they are adjacent to the latter. Away from such boundaries, however, the matrix phyllosilicates appear to be randomly oriented. We generally observe such random orientation only in rocks where detrital grains support pore space in which authigenic clay minerals crystallize independent of burial load stress, as in siltstones of the Salton Sea region (Yau *et al* 1987, Yau *et al* 1988), and the Upper Devonian Antrim shale in Michigan Basin (Hover *et al* in press). Pore space is not abundant, but where observed, it commonly is defined by the intersections of three orientations of matrix phyllosilicates, resulting in pore space with triangular shapes (Figure 4). Such relations also imply that the matrix phyllosilicates precipitated directly in pore space.

Detrital-shaped chlorite. Detrital-shaped chlorite is ubiquitous in all samples from both mineralized and unmineralized areas. The grains are very large (up to 450 × 30 μm) and have a preferred orientation with their long aspects parallel or subparallel to bedding. Grain boundaries of this chlorite display no coherent relation (i.e., they are not parallel) to surrounding matrix phyllosilicates and such grains are interpreted to be detrital in origin. TEM observations reveal that these
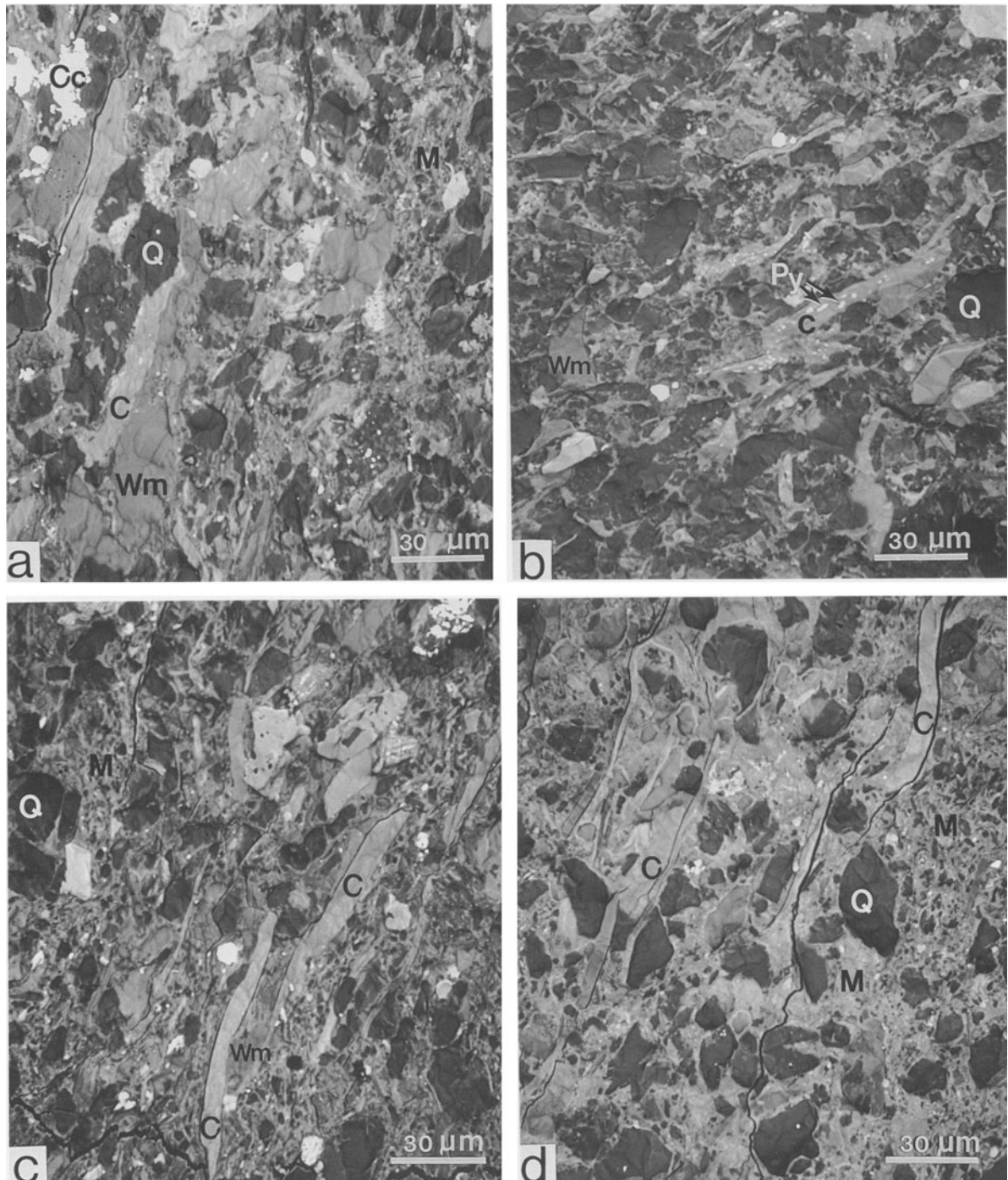
Figure 3.   Back-scattered electron (BSE) images illustrating textural relationships of studied shales. a) Sample 139, mineralized 'thinly' shale; b) Sample 511, unmineralized 'thinly' shale; c) Sample 421, mineralized 'domino' shale; d) Sample 517, unmineralized 'domino' shale. C: chlorite, Wm: white mica, Q: quartz, Ab: albite; Py: pyrite, Cc: chalcocite, M: matrix.

chlorite grains consist of aggregates of parallel to sub-parallel thick packets of 14-Å lattice fringes. Such chlorite commonly exhibits imperfections, e.g., lattice fringes are locally curved, and numerous layer termi-nations and low angle boundaries were observed (Fig-ure 5). Other SAED patterns of detrital-shaped chlorite indicate semi-random stacking disorder. In some plac-es, thick packets of chlorite with 14-Å periodicity have
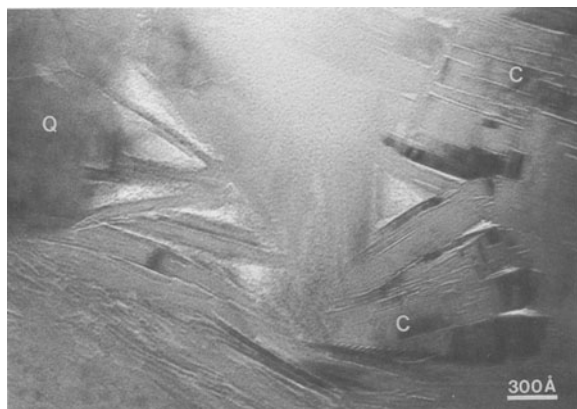
Figure 4. Low magnification TEM image showing random distribution of matrix phyllosilicates with triangular pore spaces. Sample 511, 'thinly' shale.
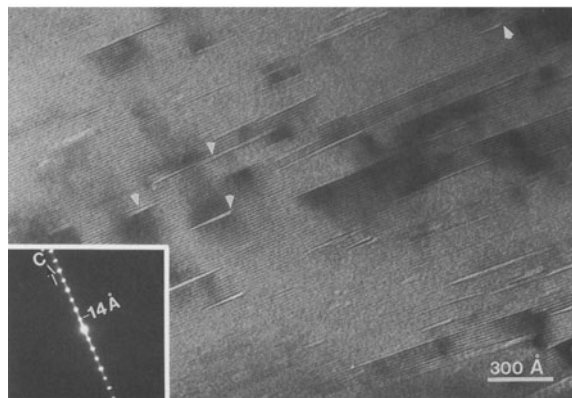

Figure 5. TEM lattice fringe image showing detrital-shaped chlorite with locally curved layers, numerous layer terminations (indicated by small arrows) and low angle grain boundaries. The corresponding SAED pattern displays diffuseness along c*. Sample 421, 'domino' shale.

some intercalated layers with 10-Å spacings, resembling chlorite with some missing interlayer hydroxide (or "brucite") sheets, consistent with diffuseness along c* in their corresponding SAED patterns. In addition, AEM analyses of such areas commonly indicate the presence of Ca and Na. The combined TEM and analytical data therefore imply that the 10-Å fringes correspond to collapsed smectite rather than mica. The 10-Å fringes intercalated within dominant chlorite locally produce 1:1 mixed-layer chlorite/smectite (corrensite) with 24-Å periodicity (Figure 6). In other cases, very thin packets (up to 70 Å thick) of white mica with 10-Å periodicity were observed interstratified with dominant 14-Å layers, forming chlorite-mica stacks (Figure 7). The features described above apply to detrital-shaped chlorite in all samples examined in this study.

Representative chemical compositions of detrital-shaped chlorite obtained from AEM analyses were normalized on the basis of 14 O atoms (c.f. Laird 1988) and are presented in Table 2. Chlorite from mineralized samples (139 and 421) commonly has a Fe/(Fe+Mg) ratio from 0.52 to 0.58 and is relatively homogeneous. However, the Fe/(Fe+Mg) ratio of chlorite in unmineralized samples (511 and 517) is quite variable, ranging from 0.12–0.52. In general, detrital-shaped chlorite from mineralized samples has higher Fe contents than detrital-shaped chlorite from unmineralized samples. However, detrital-shaped chlorite in an unmineralized sample (420) has an Fe/(Fe+Mg) ratio ranging from 0.60 to 0.70, the highest Fe content observed in chlorite by AEM in this study. All detrital-shaped chlorite contains Mn ranging from 0.02 to 0.13 per formula unit (pfu). In both mineralized and unmineralized samples, analyses of most detrital-shaped chlorites indicate significant Ti, about 0.2–0.15 pfu. In addition, analyses of almost all chlorite indicate the presence of interlayer cations Ca, Na and K, with total

Ca+Na+K contents ranging from 0.06 to 0.18 pfu. Compared to detrital-shaped chlorite in other samples, the chlorite in sample 139 contains more Na, which may reflect the presence of tiny NaCl crystals. As an interesting aside, we note the observation in TEM images and AEM analysis of NaCl crystals <1 μm in size within detrital-shaped chlorite in mineralized sample 139 but not in unmineralized sample 511 which is at the same stratigraphic horizon as sample 139. The crystals were detected in a thinned edge which had been exposed during ion milling, and which had not been affected by water during sample preparation. Because halite is soluble in the water commonly used in cutting and thinning samples, it may be much more common in Nonesuch Formation sediments than it is believed to be.

The chlorite structure generally does not accommodate Ti and interlayer cations (Deer et al 1966, Bayliss 1975) and the presence of such elements in AEM analyses of detrital-shaped chlorite is at least in part attributed to the presence of collapsed smectite (10 Å) layers. Formulae of detrital-shaped chlorite having Ti and interlayer cations also show a large range of excess Al^{VI} (up to 0.36 pfu) over Al^{IV}, as generally characteristic of low-grade metamorphic chlorite in clastic sedimentary rocks (Boles and Coombs 1977, Ramamohan Rao 1977, Evarts and Schiffman 1983, Weaver 1984, Morad 1986, Aguirre and Atherton 1987). Such relations have been shown to be directly related to the proportion of expandable layers by Shau et al (1990).

Detrital-shaped white mica. As with detrital-shaped chlorite, large flakes (up to 150 × 20 μm) of detrital-shaped white mica are oriented with their long aspects parallel or subparallel to bedding. They consist of aggregates of parallel to subparallel packets, each ranging
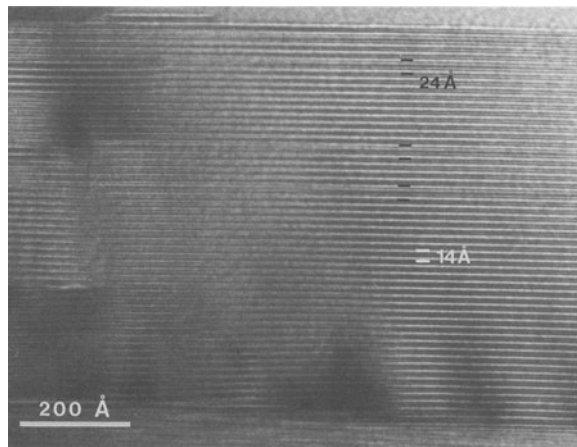
Figure 6.   TEM lattice fringe image of (001) planes of detrital-shaped chlorite shows layers with 10-Å spacing interstratified with the dominant 14-Å layers, but no two 10-Å layers are adjacent. Sample 139, 'thinly' shale.
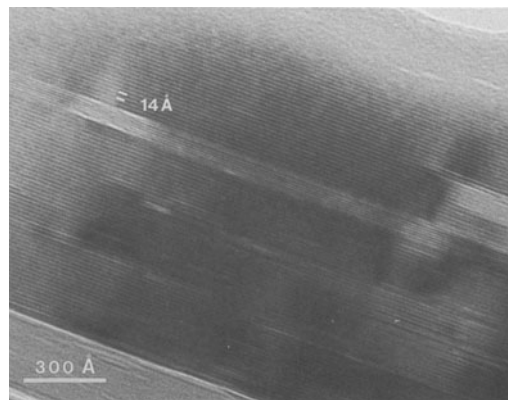

Figure 7.   TEM (001) lattice fringe image of detrital-shaped chlorite showing a packet of illite (10-Å spacing) 60 Å thick within dominant chlorite (14-Å spacing). Sample 421, 'domino' shale.

from a few hundred to a thousand angstroms in thickness. Lattice fringe images generally display 10-Å periodicities but their SAED patterns show that they are well-crystallized two-layer polytypes (Figure 8). Layer terminations and low angle boundaries are rarely observed but some wavy layers are seen in lattice fringe images (Figure 8). The "mottled" contrast displayed in lattice fringe images is characteristic of cation diffusion induced by the electron beam (Ahn and Peacor 1986).

Representative AEM analyses of detrital-shaped white mica were normalized on the basis of 12 cations on tetrahedral and octahedral sites (Table 3). Most are generally phengitic in composition, having a higher Si content (6.40–6.61 Si pfu) than muscovite and with significant Fe and Mg (total Fe+Mg ~ 0.49–0.75 pfu). The Fe/(Mg+Fe) ratio varies over a wide range (0.33–0.71). However, a white mica having a composition near that of ideal muscovite was observed in unmineralized samples 511-2 and 420-2. It has a Si/Al ratio close to 1 (with 6.03 and 6.12 Si pfu, respectively) and lower Fe and Mg (total Fe+Mg ~ 0.14 and 0.17 pfu, respectively). All detrital-shaped white micas display only slight deficiencies in interlayer cations (K+Na+Ca = 1.83–1.91 pfu) and therefore have "mature" compositions as compared with authigenic illite. Most detrital-shaped white micas contain no detectable Na and Ca except for a single sample (0.22 pfu Na, Table 3, analysis 420-2) which was collected from unmineralized strata 20 km southwest of the mine area. All detrital-shaped white micas contain a trace of Ti (0.03–0.07 pfu).

Matrix chlorite. Chlorite is the dominant phyllosilicate in the matrix of all samples. It typically occurs as continuous anastomosing units wrapped around detrital
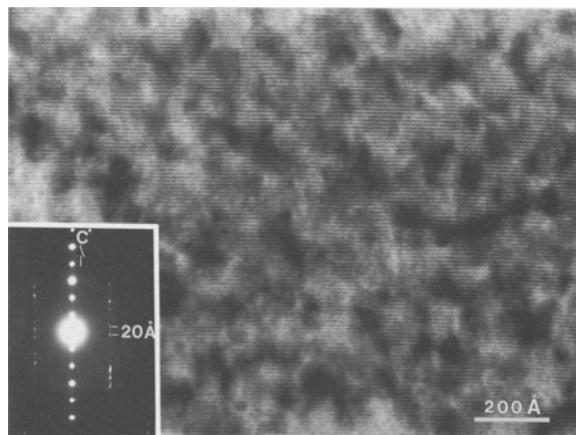

Figure 8.   Lattice fringe image of (001) planes of detrital-shaped white mica displays slightly wavy layers with 10-Å spacing. The inset corresponding SAED pattern indicates a 2-layer polytype with 20-Å periodicity. Sample 421, 'domino' shale.

grains. When not adjacent to detrital grains, its orientation is random, sometimes defining triangular pores filled with smaller chlorite packets (Figures 4 and 9). The thickness of chlorite packets varies over a large range; most are less than 200 Å thick but some are as thick as 1000 Å. Lattice fringe images of such chlorite commonly show straight, coherent layers with 14-Å periodicity. Some slightly thick packets are relatively defect free, with layer terminations being only rarely observed, although low angle boundaries between packets were commonly seen (Figure 9). Other chlorite packets display abundant defect features. For example, a lattice fringe image of such chlorite shows that layers of chlorite packets less than 200 Å thick are kinked and bent and that low angle boundaries occur between adjacent packets (Figure 10). The kink banding in Fig-

Table 2. Representative AEM analyses of chlorite.[1]

| | Detrital-shaped chlorite | | | | | | | Matrix chlorite | | | | | |
	139	421	511-1	511-2	517-1	517-2	420	139	421	421-C	511	517	420
Si	2.89	3.02	3.01	3.05	2.99	3.10	2.92	2.85	2.87	3.22	3.01	2.94	3.02
Al^{IV}	1.11	0.98	0.99	0.95	1.01	0.90	1.08	1.15	1.13	0.78	0.99	1.06	0.98
Al^{VI}	1.25	1.03	1.06	1.04	1.02	1.10	1.42	1.28	1.36	1.31	1.07	1.27	1.20
Ti	0.04	0.13	0.15	n.d.[2]	0.10	n.d.	0.02	n.d.	n.d.	n.d.	n.d.	n.d.	n.d.
Fe^{2+}	2.38	2.56	2.30	1.52	2.12	1.45	2.74	2.68	2.54	2.37	2.60	2.51	2.44
Mg	1.95	1.99	2.21	3.27	2.59	3.32	1.55	1.85	1.93	2.01	2.19	1.99	2.17
Mn	0.13	0.05	0.04	0.06	0.04	0.02	0.06	0.07	0.09	0.03	0.06	0.03	0.05
Ca	0.03	0.02	0.03	0.03	n.d.	n.d.	0.02	n.d.	n.d.	0.05	n.d.	n.d.	0.02
Na	0.07	n.d.	n.d.	0.05	n.d.	n.d.	0.02	n.d.	n.d.	0.09	n.d.	n.d.	n.d.
K	0.08	0.04	0.04	0.02	0.07	n.d.	0.09	n.d.	n.d.	0.03	n.d.	0.03	0.03
Total cations	9.93	9.82	9.83	9.99	9.94	9.90	9.92	9.88	9.92	9.89	9.92	9.83	9.91
(Ca+Na+K)	0.18	0.06	0.07	0.10	0.07	0	0.13	0	0	0.17	0	0.03	0.05
Fe/(Fe+Mg)	0.55	0.56	0.51	0.32	0.45	0.30	0.64	0.59	0.57	0.54	0.54	0.56	0.53

[1] Each formula is normalized on the basis of 14 O atoms. All Fe calculated as FeO. Two standard deviations on the basis of calculating statistics are 0.05–0.07 pfu for Si, 0.03–0.04 and 0.04–0.05 pfu for Al^{IV} and Al^{VI}, respectively, 0.20–0.25 pfu for Fe, 0.09–0.15 pfu for Mg, and 0.01–0.02 pfu for Mn.

[2] n.d. = not detectable.

ure 10 occurs presumably as the result of compaction during grain growth, as the kinking apparently took place before the growth of additional straight chlorite layers on both sides. Another lattice fringe image has abundant layer terminations, edge dislocations and split layers (Figure 11). The inset electron diffraction patterns in Figures 10 and 11 all display diffuse streaking along c* as consistent with the defects and/or disorder in the layer stacking sequence. Most matrix chlorite is either a regular 1-layer polytype or has a disordered structure characterized by sharp k = 3n reflections and streaking of k ≠ 3n reflections. In other cases, some chlorite units are bent and folded, implying modification by tectonic stress during or after their growth. For example, Figure 12a shows that a unit up to 0.25 μm thick of chlorite packets in sample 421 has been completely folded. The spread of reflections in the inset

corresponding SAED pattern demonstrates different orientations of layers in the same unit. Some grains in the same sample also display random mixed-layering of chlorite and illite as shown in Figure 12b, which is an enlargement of a part of Figure 12a. Lattice fringes shown in Figure 12b represent structural layers of illite and dominant chlorite with periodicities of 10 and 14 Å, respectively. Regions of 1:1 ordered mixed-layering of chlorite/collapsed smectite can be seen with 24 Å periodicity, forming corrensite-like layers, although the 1:1 ordering is limited only to small regions. Locally, two or three 10-Å illite layers are adjacent, forming thin packets (Figure 12b).

Representative chemical compositions of matrix chlorite, as measured by AEM analysis, are also shown in Table 2. The matrix chlorite in mineralized samples (139 and 421) has a range of Fe/(Fe+Mg) ratios from

Table 3. Representative AEM analyses of white mica[1].

| | Detrital-shaped white mica | | | | | | | Matrix illite-rich I/S | | | | |
	139	421	511-1	511-2	517	420-1	420-2	139	421	511	517	420
Si	6.40	6.59	6.45	6.03	6.61	6.44	6.12	7.24	7.26	7.32	7.29	7.20
Al^{IV}	1.60	1.41	1.55	1.97	1.39	1.56	1.88	0.76	0.74	0.68	0.71	0.80
Al^{VI}	3.23	3.35	3.35	3.81	3.19	3.44	3.80	3.25	3.28	3.16	3.14	3.20
Ti	0.06	0.04	0.05	0.05	0.06	0.07	0.03	n.d.[2]	n.d.	n.d.	n.d.	n.d.
Fe^{2+}	0.26	0.31	0.20	0.10	0.32	0.33	0.09	0.38	0.36	0.47	0.53	0.41
Mg	0.45	0.30	0.40	0.04	0.43	0.16	0.08	0.37	0.36	0.37	0.33	0.39
Ca	n.d.	n.d.	n.d.	n.d.	n.d.	n.d.	n.d.	n.d.	n.d.	n.d.	n.d.	n.d.
Na	n.d.	n.d.	n.d.	n.d.	n.d.	n.d.	0.22	n.d.	n.d.	n.d.	n.d.	n.d.
K	1.90	1.89	1.83	1.88	1.86	1.91	1.62	1.07	1.21	1.10	1.18	1.26
Total cations	13.90	13.89	13.83	13.88	13.86	13.91	13.84	13.07	13.21	13.10	13.18	13.26
NNC[3]	2.19	1.94	2.05	2.01	2.02	1.91	1.99	1.51	1.46	1.52	1.57	1.60
Fe/(Fe+Mg)	0.37	0.52	0.33	0.71	0.43	0.67	0.53	0.50	0.50	0.56	0.62	0.52

[1] Each formula is normalized on the basis of 12 cations on tetrahedral and octahedral sites. All Fe calculated as FeO. Two standard deviations on the basis of calculating statistics are 0.11–0.14 pfu for Si, 0.03–0.05 and 0.08–0.09 pfu for Al^{IV} and Al^{VI}, respectively, 0.01 pfu for Ti, 0.01–0.03 pfu for Fe, 0.01–0.02 pfu for Mg, 0.01–0.04 pfu for Na, and 0.06–0.13 pfu for K.

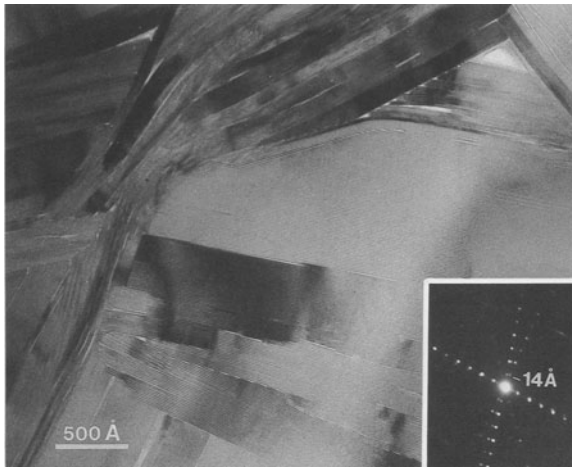[2] n.d. = not detectable.

[3] Net negative charge.

Figure 9. Lattice fringe image of (001) planes of matrix chlorite and corresponding diffraction pattern show different orientations of chlorite packets whose intersections define triangular pore space. Some packets locally display straight and coherent defect-free fringes although low angle boundaries between packets are also present. Sample 420.
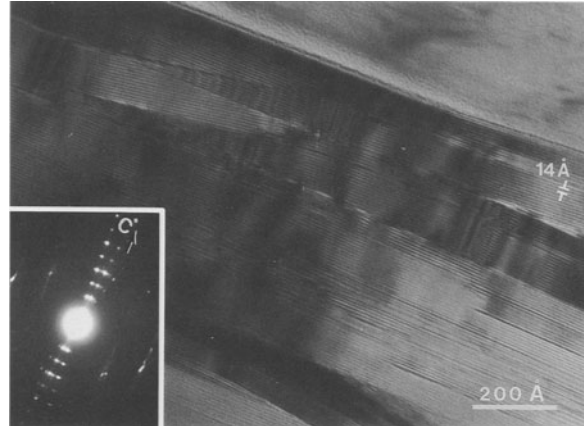

Figure 10. Lattice fringe image of (001) planes of matrix chlorite showing kinking and bending of the layers. The inset corresponding SAED pattern is diffuse along c*. Sample 420.

0.52 to 0.60, slightly more enriched in Fe than detrital-shaped chlorite. In unmineralized samples, the Fe/(Fe+Mg) ratio of matrix chlorite from the 'thinly' (511) and 'domino' (517) shale samples ranges from 0.50 to 0.63, values that are much higher than those of detrital-shaped chlorite in the same samples, although the matrix chlorite surrounding Fe-rich detrital-shaped chlorite generally has slightly higher Fe contents than matrix chlorite surrounding Fe-poor detrital-shaped chlorite. Generally speaking, matrix chlorite is relatively Fe-rich compared with detrital-shaped chlorite except in sample 420. In sample 420, which was collected from unmineralized 'upper' Nonesuch Formation strata 20 km southwest of the mine, the Fe/(Fe+Mg) ratio of matrix chlorite ranges from 0.47 to 0.60, slightly less than that of detrital-shaped chlorite in the same sample. However, the Fe/(Fe+Mg) ratios of matrix chlorite in all samples are still in the range of 0.47 to 0.63, and the matrix chlorite is relatively homogeneous compared with detrital-shaped chlorite in all samples. In contrast with detrital-shaped chlorite, none of the matrix chlorite contains Ti and Na and most analyses of such chlorite do not contain Ca and K. The small amount of Ca (0.02 pfu in sample 420) and K (0.03 pfu in samples 517 and 420) in some chlorite from unmineralized samples may reflect interlayered 10-Å layers (collapsed smectite) or contamination by surrounding minerals. Although the formulae of matrix chlorite show a relatively smaller range of excess Al^{VI} (0.08 to 0.23 pfu) over Al^{IV} compared to that (up to 0.36 pfu) of detrital-shaped chlorite, the range of excess Al^{VI} of the former is still characteristic of diagenetic or low-grade metamorphic chlorite in clastic sedimentary

rocks (e.g., Weaver 1984, Morad 1986, Aguirre and Atherton 1987).

The chemical composition of random mixed-layer smectite with chlorite (corrensite-like) material has also been analyzed by AEM (analysis 421-C in Table 2). It has a higher Si/Al ratio and more excess Al^{VI} (up to 0.53 pfu) relative to Al^{IV} than chlorite. Its Fe/(Fe+Mg) ratio is approximately 0.54, similar to that of matrix chlorite. It contains significant Ca, Na, and K (Ca+Na+K = 0.17 pfu) as interlayer cations. Approximately 0.03 pfu Mn was detected in this material, but Ti is absent.

Matrix illite-rich I/S. Because XRD data indicated that there is a measurable expandable-smectite interlayer component to I/S, the sample with the largest smectite component (WPB 420) was treated with L. R. White
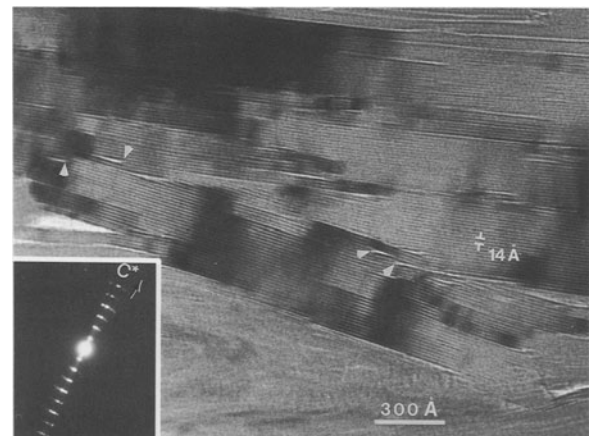

Figure 11. Lattice fringe image of (001) planes of matrix chlorite showing abundant layer terminations (edge dislocations; indicated by small arrows) and low angle boundaries. The inset corresponding SAED pattern also shows diffuseness along c*. Sample 511, 'thinly' shale.
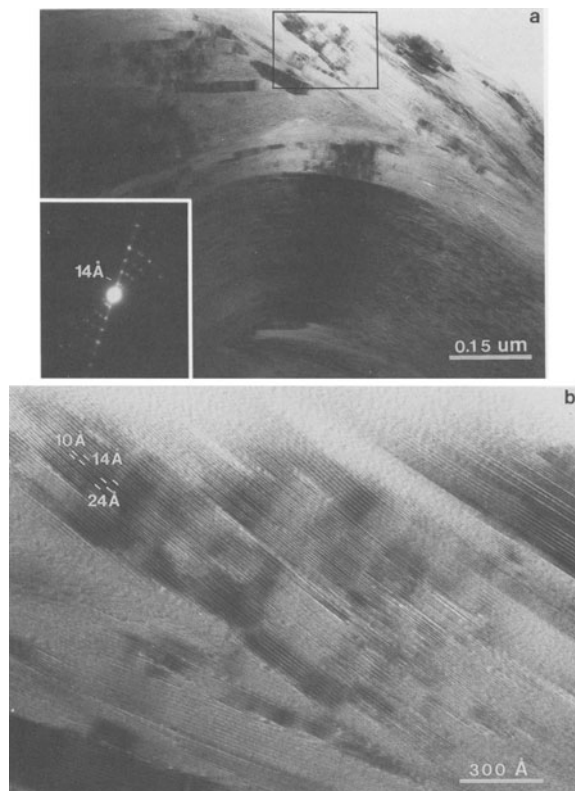
Figure 12. Lattice fringe image of (001) planes of matrix chlorite. (a) Low magnification bright field image shows that a unit (up to 0.25 μm thick) of matrix chlorite packets was severely deformed. The inset corresponding SAED pattern demonstrates different orientations of layers in the same unit and diffuseness along the c* axes. (b) An enlargement of part of (a) shows that straight layers with 10-Å spacing are interstratified within the dominant 14-Å layers. The 10-Å layers occur as only one, or two to three layers adjacent layers. Where single layers occur, they form 24-Å corrensite-like units with adjacent 14-Å chlorite layers. Sample 421, 'domino' shale.
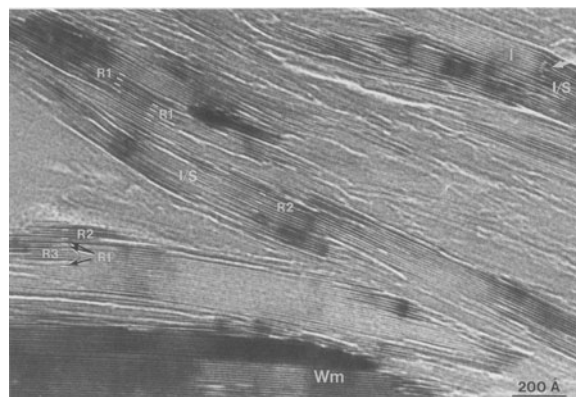

Figure 13. TEM lattice fringe image of (001) planes of illite-rich I/S in a permanently expanded shale sample (Sample 420). Relatively straight layers are illite with 10-Å periodicity whereas those slightly wavy lattice fringes with slightly larger d-spacings ($\sim$11–11.5 Å) correspond to smectite layers. In some areas, contrast of ordered I/S corresponding to R1 (with $\sim$21–21.5 Å periodicity), R2 (with $\sim$31–32 Å periodicity), and R3 (with $\sim$41–42 Å periodicity) I/S can be observed. Edge dislocation and other crystal defects are commonly seen in I/S. I: illite, I/S: mixed-layer illite and smectite, Wm: detrital-shaped white mica.

resin to cause permanent expansion of smectite-like interlayers so that they can be differentiated from illite-like interlayers in lattice fringe images (Kim *et al* 1995). The resulting lattice fringe images show that most fine-grained illite occurring in the matrix occurs as thin packets of layers with 10-Å periodicity; that is, it is illite, sensu strictu. However, some lattice fringes are slightly wavy compared to illite fringes, and have d(001) values larger than 10 Å. Such fringes are therefore interpreted to correspond to smectite interlayers. In some cases, contrast in lattice fringes of ordered I/S corresponding to R1 ($\sim$21–21.5 Å periodicity), R2 ($\sim$31–32 Å periodicity), or R3 ($\sim$41–42 Å periodicity) I/S was observed. Such I/S minerals commonly display edge dislocations and other crystal defects (Figure 13). Measurement of the proportion of smectite layers in I/S showed that there are approximately 20–30% expandable interlayers, as consistent with the XRD data

of Price and McDowell (1993). Although only sample 420 was treated so that expanded smectite-like interlayers could be observed, we infer that the satisfactory results for that sample are representative of the others, and we therefore refer to such material generally as "illite-rich I/S."

Illite-rich I/S is generally subordinate to chlorite in the matrix of all samples. It occurs as thin packets of layers that are commonly closely associated with matrix chlorite. Most illite-rich I/S packets are less than 200 Å thick and are locally as thin as 30 Å. As is the case for chlorite, matrix illite-rich I/S appears to be randomly oriented relative to bedding. Lattice fringe images commonly show parallel or subparallel packets bordered by low-angle grain boundaries with chlorite packets. Illite-rich I/S may have straight or slightly wavy layers with 10-Å periodicity and contain high concentrations of layer terminations (e.g., Figure 14). The inset corresponding SAED pattern in Figure 14 shows that illite-rich I/S coexisting with matrix chlorite (14-Å layers) is a disordered $1M_d$ polytype with 10-Å periodicity. Although matrix illite-rich I/S is rarely observed compared to matrix chlorite, all SAED patterns of illite-rich I/S display 10-Å periodicity in 001 reflections but with diffuse streaking along c* in non-001 rows as consistent with stacking disorder.

Table 3 also lists the representative compositions of illite-rich I/S in all samples as determined by AEM analysis. The data were obtained only from areas demonstrated by TEM to be single phases. Compared to ideal muscovite and detrital-shaped white mica, all illite-rich I/S has a relatively high Si/Al ratio, a higher

content of Fe+Mg (0.75–0.86 pfu) and lower total of interlayer cations (1.07 to 1.26 pfu). No Ti, Ca, or Na were detected in the illite-rich I/S. The Fe/(Fe+Mg) ratios of illite-rich I/S are approximately 0.50 to 0.62, similar to those of matrix chlorite. The net negative charges range from 1.46 to 1.60 pfu when all Fe is calculated as ferrous. However, if all Fe is calculated as ferric, the net negative charges vary from 1.02 to 1.19 pfu. Such compositions correspond to authigenic illite rather than to evolved micas because in the former the net negative charges are equal to or less than 1.6 (Šrodoń et al 1986, Jiang et al 1992).

DISCUSSION

Origin of detrital-shaped phyllosilicates

The morphology and grain size of detrital-shaped phyllosilicates, their general parallelism with bedding, and textural relationships with matrix phyllosilicates collectively imply that the detrital-shaped chlorite and white mica were originally detrital grains.

TEM lattice fringe images of detrital-shaped chlorite show that some 10-Å collapsed smectite layers occur interlayered with the dominant 14-Å chlorite layers, forming random mixed-layering of 14-Å layers with 10-Å layers, i.e., forming 24-Å corrensite-like units. In other cases, thin packets of 10-Å layers (mica-like) are intergrown with thick packets of chlorite, constituting chlorite-mica stacks. BSE images demonstrate that abundant titanium oxide grains occur within or surrounding the detrital-shaped chlorite, but not in other associations. In addition, detrital-shaped chlorite is unusual in that AEM analysis indicate the presence of considerable Ti and K. Lastly, the chlorite has a narrow range of compositions incompatible with the normal ranges for detrital chlorite, but consistent with equilibration with a pervasive pore fluid. All of these relations imply that detrital volcanic biotite, which is characterized by the presence of Ti, was a precursor of detrital-shaped chlorite, as found in other studies (White et al 1985, Dimberline 1986, Jiang 1993). Although no remnants of biotite were observed in the White Pine shales due to complete alteration during diagenesis, biotite has been found in association with chlorite in the Nonesuch shales in Wisconsin (Kim and Peacor, unpublished data), where the formation temperature of clays has been shown to be lower and I/S expandability to be higher than those of clays in the White Pine area (Price and McDowell 1993). The precursor of at least much of the detrital-shaped chlorite is therefore inferred to have been volcanic biotite derived from the volcanic detritus which forms a substantial part of the sediment input to the Midcontinent Rift Basin. Other chlorite may have been formed by replacement of pumice fragments or volcanic glass (e.g., Boles and Coombs 1977).

Direct alteration of biotite to chlorite during diagenesis and low-grade metamorphism has been described
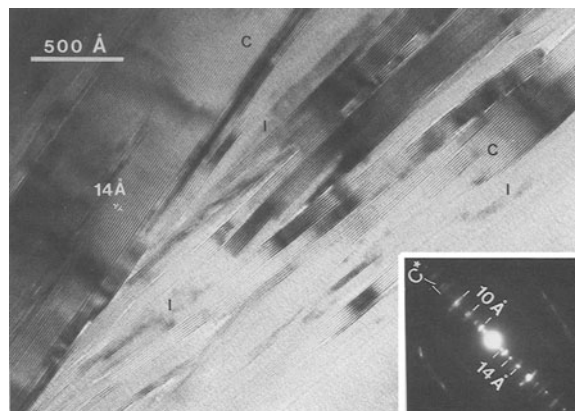

Figure 14. Lattice fringe image of (001) planes of matrix illite-rich I/S and coexisting chlorite shows that illite-rich I/S occurs as straight layers of packets less than 150 Å thick. The inset corresponding diffraction pattern shows that the illite-rich I/S is a disordered $1M_d$ polytype with 10-Å periodicity. Sample 511, 'thinly' shale.

by a number of workers (e.g., Ferry 1978, 1979, Veblen and Ferry 1983, AlDahan and Morad 1986, Morad 1986, Morad and AlDahan 1986). Replacement of biotite by chlorite through progressive alteration of biotite layers into chlorite layers has been demonstrated by TEM observations in many cases (e.g., Banos et al 1983, Veblen and Ferry 1983, Eggleton and Banfield 1985, Jiang 1993). Biotite has also been demonstrated to be replaced by expandable, trioctahedral phyllosilicates which may subsequently be directly replaced by chlorite in prograde sequences. The alteration of ferromagnesian minerals, including biotite, to expandable trioctahedral phyllosilicates has been shown to be one of the earliest water/rock hydration reactions to occur following the eruption of volcanic rocks (April and Keller 1992). For example, Kisch (1983), Curtis et al (1985), Eggleton and Banfield (1985), and Ilton and Veblen (1988) have demonstrated vermiculite, smectite, or hydrobiotite replacements of biotite. TEM/AEM data of Jiang (1993) showed that both corrensite and chlorite initially replaced volcanic biotite, with the expandable component having subsequently been replaced by chlorite during prograde metamorphism of pelites. Initially therefore, biotite may have been altered to vermiculite or trioctahedral smectite and through corrensite to chlorite during the formation of the detrital-shaped chlorite. The presence of corrensite-like layers and mixed-layering of 10-Å layers in the detrital-shaped chlorite observed in this study is consistent with such a sequence, and further supports the conclusion that detrital biotite was the precursor.

As observed in SEM images, detrital-shaped white micas are oriented parallel to bedding, but are commonly distorted and bent around quartz grains. No evidence at any level (optical, SEM, or TEM) was found

to indicate that detrital-shaped white mica grains had recrystallized or formed by alteration of other minerals. Their compositions, polytypism, and defect-free nature are consistent with characteristics of mature micas inherited from higher grade rocks.

Formation of matrix clay minerals

Matrix chlorite occurs ubiquitously as thin packets of layers with subordinate illite (or I/S) that display no preferred orientation, but form continuous, anastomosing arrays that wrap around detrital-like grains. At the TEM scale, these thin packets display various growth defects such as layer terminations, edge dislocations, and kink banding due to compaction during crystal growth. Single chlorite or illite layers are observed as mixed layers within illite or chlorite packets, respectively. Illite or I/S has a relatively high Si/Al ratio, a high content of Fe+Mg and a low total of interlayer cations (all K, about 1.07 to 1.26 pfu) compared with muscovite. On the other hand, matrix chlorite in all samples is relatively Fe-rich with a Fe/(Fe+Mg) ratio ranging from 0.47 to 0.63, similar to authigenic chlorite from other localities (Curtis *et al* 1985). The high Fe content of chlorite formed during diagenesis has also been stressed by many other workers (e.g., Hayes 1970, Velde *et al* 1974, Velde 1977, Lee *et al* 1984, Dimberline 1986, Hillier and Velde 1991).

The chemical compositions and textural relationships of matrix clays with detrital-shaped grains are very similar to those of Gulf Coast shales and low grade sediments of the Gaspé Peninsula, Québec. For example, I/S that has formed directly by a transformation in which smectite is a reactant is enriched in Si, Fe and Mg, but depleted in Al and K relative to muscovite (Boles and Frank 1979, Ahn and Peacor 1986), and chlorite has a high Fe/(Fe+Mg) ratio in Gulf Coast shales (Ahn and Peacor 1985). Thin packets of authigenic illite (or I/S) and chlorite occur as anastomosing arrays that wrap around detrital grains, and matrix clays are characterized by various growth defects such as layer terminations, edge dislocations, and kink banding due to compaction in Gulf Coast shales (Lee *et al* 1985, Ahn and Peacor 1986) and pelitic rocks of the lower diagenetic zone in Québec (Jiang 1993). These data are consistent with derivation of matrix clays in the Nonesuch Formation through dissolution of detrital smectite and crystallization of primary chlorite and I/S. As smectite transforms to illite as a function of burial depth in Gulf Coast shale, there is a large increase in K and Al, but a decrease in Si, Fe and Mg in illite. Coexisting chlorite may have formed at the same time as a by-product of the reaction, with Fe and Mg released from the breakdown of smectite layers being a major source of cations for authigenic chlorite (Perry and Hower 1970, Hower *et al* 1976). Textural relations of matrix illite and chlorite observed in this study are similar to the chlorite and illite relations in Gulf Coast

shales (Ahn and Peacor 1985), implying that at least some of the chlorite formed as a result of the larger Fe and Mg contents of reactant smectite as compared to product illite.

In contrast to the dominant dioctahedral I/S minerals in Gulf Coast sediments, however, trioctahedral chlorite and mixed-layer chlorite/trioctahedral smectite are common in Nonesuch shales. This is ascribed to different bulk rock compositions, because compared to the more felsic sediments of the Gulf Coast, original Nonesuch sediments had a higher proportion of basaltic volcanic materials. Weathering and alteration of such Fe- and Mg-rich volcanic material therefore led eventually to the formation of dominant chlorite. In this respect, Nonesuch shales resemble the Gaspé Peninsula metasediments which had a significant mafic volcanogenic component, and further demonstrate that where low-grade metasediments are derived largely from volcanic precursors, the chlorite/white mica ratio may vary over wide limits in response to the ratio of basaltic and felsic components (Jiang, 1993).

The TEM/AEM characteristics of matrix phyllosilicates in the Nonesuch Formation are typical of immature clays that formed in the earliest stages of prograde sequences of pelites, as reviewed by Peacor (1992). These characteristic include crystal size, crystal heterogeneity, crystal defects, and polytypism. (1) Crystal size. Packets a few tens of angstroms in thickness, such as those in the matrix of the Nonesuch Formation, are typical of clay minerals that have transformed from smectite at the lowest grades of diagenesis, and that have not been further modified. The thickness of early-formed packets of clays increases with increasing grade (e.g., Merriman *et al* 1990, Jiang 1993). (2) Crystal heterogeneity. Matrix clay minerals of the Nonesuch Formation are heterogeneous in both composition and structure. Chemically, although individual packets of clay minerals are relatively homogeneous in composition, adjacent packets vary widely in composition. This is a fundamental condition of chemical non-equilibrium which is common in early diagenetic sequences. Structurally, matrix white mica is illite-rich I/S, occurring as various ordered mixed-layering of illite and smectite, rather than pure mature illite. On the other hand, corrensite mixed-layers occur within chlorite, apparently as a relict of more abundant corrensite layers that formed at lower grades, whereas individual illite and chlorite layers occur within packets of chlorite and illite, respectively. Such mixed-layer crystals are metastable. (3) Crystal defects. Matrix clay minerals were observed to have high concentrations of layer terminations, edge dislocations, and kinking due to compaction during crystal growth. Elsewhere, Lee *et al* (1984, 1986) noted that early-formed chlorite and illite have higher concentrations of defects, while Livi *et al* (1988) observed that poorly-crystalline illite generally has higher concentrations of interlayer vacancies.

(4) Polytypism. Illite or I/S are generally disordered in stacking sequence, with diffuse, ill-defined non-001 reflections, a feature Grubb et al. (1991) noted as typical of illite in its original state as a transformation product of primary smectite. Similarly, matrix chlorite is a 1-layer structure with stacking disorder, a metastable state inferred by Bailey and Brown (1962) and Hayes (1970) to transform to a more stable state with increasing temperature.

The above features collectively demonstrate that matrix chlorite and illite-rich I/S in Nonesuch shales have not undergone subsequent transformation to mature phyllosilicates despite their great age of over 1 Ga. Lack of modification of such clays over such an extensive interval of time emphasizes their ability to retain metastable states when they are unaffected by factors such as pore fluids and tectonic stress that promote reactions in which products approach equilibrium states.

Homogenization of detrital phyllosilicates within the ore-body

The proportion (up to 30%) of detrital-shaped chlorite in shales and siltstones of the Nonesuch Formation is extremely high. Optical and SEM studies of such rocks described by others (e.g., Sliney, 1988) and in this study reveal that sulfides in phyllosilicates occur only in chlorite. In mineralized samples, elongated chalcocite inclusions are observed to occur along the (001) lens-shaped voids occurring along layers of detrital-shaped chlorite but not within detrital-shaped white mica, whereas in unmineralized samples, the relation involves pyrite in detrital-shaped chlorite. This implies that precipitation of Fe and Cu sulfides was controlled by a localized chemical environment associated with chlorite.

Ilton and Veblen (1988) observed that anomalous Cu occurs as flattened submicroscopic inclusions oriented parallel to the locally separated layers of enclosing mixed-layer phyllosilicates which form by alteration of biotite to expandable trioctahedral clays in porphyry copper deposits and in experimental run products (Ilton et al 1992). They concluded that phyllosilicates act as sinks for Cu mineralization. In the Nonesuch Formation, many authors have suggested that pyrite developed first and that later, some of the pyrite crystals were replaced by copper sulfides, with detrital-shaped chlorite also acting as a sink for the Cu-mineralization. This replacement-mineralization process was inferred to have been promoted by a cupriferous-chloride brine migrating upward through the underlying Copper Harbor Conglomerate (e.g., Brown 1971, White 1971, Wiese 1973), as evidenced in part by fluid escape structures filled with chalcocite and native copper (Mauk et al 1992) and by the small cubic halite inclusions found in detrital-shaped chlorite in mineralized samples.
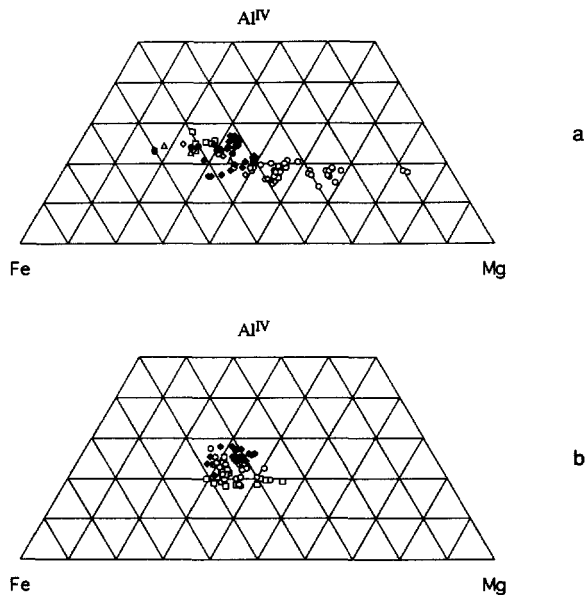

Figure 15. Plots of compositions in the ternary system Al^{IV}-Fe-Mg. (a) Detrital-shaped chlorite. (b) Matrix chlorite. Open symbols: unmineralized samples; solid symbols: mineralized samples.

AEM analyses show that detrital-shaped chlorite in mineralized samples is relatively Fe-rich compared with detrital-shaped chlorite in unmineralized samples in the same stratigraphic interval. This relationship has also been indicated in a previous mineralogical and geochemical study on a vertical comparison of Nonesuch shales by Wiese (1973). The compositions of detrital-shaped chlorite are displayed in the ternary system Al^{IV}–Fe^{VI}–Mg^{VI} in Figure 15a. These data include AEM analyses of the units described above and microprobe analyses of detrital-shaped chlorite in both mineralized and unmineralized samples from other localities, with all microprobe data of detrital-shaped chlorite obtained from analyses with Al^{VI}–$Al^{IV} < 0.4$ on the basis of normalization to 14 O atoms. There is almost no change in Al^{IV} of detrital-shaped chlorite from unmineralized to mineralized samples. However, the Fe/(Fe+Mg) ratios of detrital-shaped chlorite in unmineralized samples extend over a large range (0.15–0.75), with most values between 0.27 and 0.54; by contrast, the Fe/(Fe+Mg) ratios of detrital-shaped chlorite of mineralized samples fall in a very narrow range of 0.50–0.67, with the exception of a small number with values as large as 0.78. The narrower range in Fe/(Fe+Mg) values for detrital-shaped chlorite in mineralized samples suggests that the detrital-shaped chlorite in the ore zone has been homogenized by interaction with a pervasive fluid, presumably by those fluids that gave rise to the copper mineralization. If such homogenization was truly affected by the circulation of ore-forming fluids, the compositions of matrix

chlorite would be expected to have a narrower range similar to that of detrital-shaped chlorite. As shown in Figure 15b. matrix chlorite does indeed have a narrow range of Fe/(Fe+Mg) ratios, with values for matrix chlorite in mineralized samples plotting within the range of compositions of detrital-shaped chlorite in mineralized samples.

Mauk and Hieshima (1992) discussed the relationship between Cu mineralization and the presence and maturity of organic matter in the Nonesuch Formation. They concluded that inclusions of petroleum and pyrobitumen in calcite veins were probably derived from more deeply buried portions of the Nonesuch Formation, and that petroleum migrated into the White Pine region synchronously with thrusting. Ohr (1993) obtained U-Pb, Rb-Sr, and Sm-Nd isotope ages of carbonate and argillaceous rocks in the Nonesuch Formation. The U-Pb ratios of the Junior Limestone indicated that the isotopic composition of the mineralized total whole rock fraction has been homogenized, and that the initial Pb isotopic composition represents a reservoir slightly more radiogenic in ^{207}Pb* than defined by a range of Portage Lake basaltic rocks, suggesting the incorporation of Pb derived from an older crustal source into the mineralized bulk sedimentary reservoir. Similarly, the non-radiogenic initial ^{87}Sr/^{86}Sr of unmineralized shale assemblages is similar to that of mafic source rocks, but mineralized assemblages contain more radiogenic initial ^{87}Sr/^{86}Sr, implying that the mineralized part of the Nonesuch shale has undergone significant water-rock interaction compared to the unmineralized area. On the other hand, the initial Nd isotopic compositions of the mineralized samples is less radiogenic than that of the unmineralized samples, suggesting that the unmineralized clastic rocks are more compatible with their source rocks, and that Cu-mineralization resulted from hydrothermal circulation involving older Keweenawan rocks or underlying basement. All of these relations are consistent with the higher and more restricted range of Fe/Fe+Mg ratio of both detrital-shaped and matrix chlorites in mineralized samples compared to unmineralized samples. These relations further support the hypothesis that the detrital-shaped chlorite of mineralized samples has been homogenized by the fluids causing copper mineralization, presumably by the circulation of brines which interacted with the older rocks underlying the Nonesuch Formation.

CONCLUSION

Sediments of the 'lower' Nonesuch Formation in the Lake Superior portion of the Midcontinent rift system contain matrix clay minerals that are similar to relatively immature phyllosilicates formed during early diagenesis, including $1M_d$ illite-rich I/S and one-layer chlorite polytypes with stacking disorder. These immature clays occur in Precambrian (1.1 Ga) sediments

that host a major hydrothermal ore deposit, and have remained essentially unmodified in metastable states of formation despite their great age. This implies that clay minerals have an ability to retain metastable states when not exposed to significant pore fluids and/or tectonic stress, independent of time.

Chlorite grains with shapes characteristic of a detrital origin are inferred to have been originally deposited as volcanic biotite that altered during diagenesis. Chemical homogeneity characterizes detrital-shaped chlorites in the 'lower' Nonesuch Formation in the area of the White Pine mine, with Fe/Fe+Mg ratios of 0.52 to 0.58. Unmineralized samples collected away from the mine have Fe/Fe+Mg ratios of 0.29 to 0.64. The observed zonation in the chemical composition of detrital-shaped chlorites is consistent with the hypothesis that the White Pine hydrothermal system has an alteration halo that is characterized, at least in part, by chemically homogeneous chlorite. Presumably, high water-rock ratios drove chlorite homogenization reactions in the vicinity of the White Pine ore body, because other workers (e.g., Price and McDowell 1993) have documented only minor changes in the inferred regional paleotemperatures of this portion of the Midcontinent rift system. However, the observed change in chlorite composition occurs over a lateral distance that exceeds 60 km, so we can not preclude an alternative hypothesis that the observed zonation results from variations inherited from different sedimentary provinces.

ACKNOWLEDGMENTS

REFERENCES

Aguirre, L., and M. P. Atherton. 1987. Low-grade metamorphism and geotectonic setting of Macuchi Formation, western Cordillera of Ecuador. *J. Metam. Geol.* **5**: 473–494.

Ahn, J. H., and D. R. Peacor. 1985. Transmission electron microscopic study of diagenetic chlorite in Gulf Coast argillaceous sediments. *Clays & Clay Miner.* **33**: 228–236.

Ahn, J. H., and D. R. Peacor. 1986. Transmission and analytical electron microscopy of the smectite-to-illite transition. *Clays & Clay Miner.* **34**: 165–179.

AlDahan, A. A., and S. Morad. 1986. Chemistry of detrital

biotites and their phyllosilicate intergrowths in sandstones. *Clays & Clay Miner.* **34**: 539–548.

April, R. H., and D. M. Keller. 1992. Saponite and vermiculite in amygdules of the Granby basaltic tuff, Connecticut Valley. *Clays & Clay Miner.* **40**: 22–31.

Arehart, G. B. 1992. Age and fluid chemistry of sediment-hosted disseminated gold deposits in the Great Basin, Nevada: Ph.D. thesis. University of Michigan, Ann Arbor, Michigan, 163 pp.

Bailey, S. W., and B. E. Brown. 1962. Chlorite polytypism: I. Regular and semi-random one-layer structures. *Amer. Mineral.* **47**: 819–850.

Banos, J. O., M. Amouric, C. Fouquet, and A. Baronnet. 1983. Interlayering and Interlayer slip in biotite as seen by HRTEM. *Amer. Mineral.* **68**: 754–758.

Bayliss, S. W. 1975. Nomenclature of the trioctahedral chlorites. *Can. Mineral.* **13**: 178–180.

Boles, J. R., and D. S. Coombs. 1977. Zeolite facies alteration of sandstones in the Southland syncline, New Zealand. *Amer. J. Sci.* **277**: 982–1012.

Boles, J. R., and S. G. Frank. 1979. Clay diagenesis in the Wilcox sandstones of southwest Texas: Implications of smectite diagenesis on sandstone cementation. *J. Sed. Petrol.* **49**: 55–70.

Brown, A. C. 1971. Zoning in the White Pine copper district, Ontonagon County, Michigan. *Econ. Geol.* **66**: 543–573.

Cannon, W. F., and S. W. Nicholson. 1992. Revisions of stratigraphic nomenclature within the Keweenawan Supergroup of Northern Michigan. *U.S. Geol. Surv. Bull.* **1970**: A1–A8.

Cannon, W. F. 1989. The north American Midcontinent Rift beneath Lake Superior from GLIMPCE seismic reflection profiling. *Tectonics* **8**: 305–332.

Chase, C. G., and T. H. Gilmer. 1973. Precambrian plate tectonics: The midcontinent gravity high. *Earth Planet Sci. Letters* **21**: 70–78.

Cliff, G., and G. W. Lorimer. 1975. The quantitative analysis of thin specimens. *J. Microscopy* **103**: 203–207.

Curtis, C. D., C. R. Hughes, J. A. Whiteman, and C. K. Whittle. 1985. Composition variation within some sedimentary chlorite and some comments on their origin. *Mineral. Mag.* **49**: 375–386.

Daniels, P. A. 1982. Upper Precambrian sedimentary rocks, Oronto Group, Michigan–Wisconsin. In Geology and tectonics of the Lake Superior Basin. *Geol. Soc. Amer. Mem.* **156**: 107–133.

Deer, W. A., R. A. Howie, and J. Zussman. 1966. *An Introduction to the Rock Forming Minerals.* London: Longman Group Ltd., 528 pp.

Dimberline, A. J. 1986. Electron microscope and electron microprobe analysis of chlorite-mica stacks in the Wenlock turbidites, mid Wales, U.K. *Geol. Mag.* **123**: 299–306.

Eggleton, R. A., and J. F. Banfield. 1985. The alteration of granitic biotite to chlorite. *Amer. Mineral.* **70**: 902–910.

Elmore, R. D., G. J. Milavec, S. W. Imbus, and M. H. Engel. 1989. The Precambrian Nonesuch Formation of the North American Mid-continent Rift, sedimentology and organic geochemical aspects of lacustrine deposition. *Precambrian Research* **43**: 191–213.

Essene, E. J., and D. R. Peacor. 1995. Clay mineral thermometry—A critical perspective. *Clays & Clay Miner.* (in press).

Evarts, R. C., and P. Schiffman. 1983. Submarine hydrothermal metamorphism of the Del Puerto ophiolite, California. *Amer. J. Sci.* **283**: 289–340.

Ferry, J. M. 1978. Fluid interaction between granite and sediment during metamorphism, south-central Maine. *Amer. J. Sci.* **278**: 1025–1056.

Ferry, J. M. 1979. Reaction mechanisms, physical condi-

tions, and mass transfer during hydrothermal alteration of mica and feldspar in granitic rocks from south-central Maine, USA. *Contrib. Mineral. Petrol.* **68**: 125–139.

Grubb, S. M. B., D. R. Peacor, and W.-T. Jiang. 1991. Transmission electron microscopy observations of illite polytypism. *Clays & Clay Miner.* **39**: 540–550.

Hayes, J. B. 1970. Polytypism of chlorite in sedimentary rocks. *Clay & Clay Miner.* **18**: 285–306.

Hillier, S., and B. Velde. 1991. Octahedral occupancy and the chemical composition of diagenetic (low-temperature) chlorites. *Clay Miner.* **26**: 149–168.

Hite, D. M. 1968. Sedimentology of the upper Keweenawan sequence of northern Wisconsin and adjacent Michigan: Ph. D. thesis. University of Wisconsin, Madison, Wisconsin, 217 pp.

Hover, V. C., D. R. Peacor, and L. M. Walter. 1995. STEM evidence for preservation of diagenetic fabrics in Devonian Shales: Implications for fluid/rock interaction in cratonic basins. *J. Sedim. Res.* (in press).

Hower, J., E. V. Eslinger, M. E. Hower, and E. A. Perry. 1976. Mechanism of burial metamorphism of argillaceous sediments: 1. Mineralogical and chemical evidence. *Bull. Geol. Sci. Amer.* **87**: 725–737.

Ilton, E. S., and D. R. Veblen. 1988. Copper inclusions in sheet silicate from porphyry Cu deposits. *Nature* **334**: 516–518.

Ilton, E. S., D. Earley III, D. Morazas, and D. R. Veblen. 1992. Reaction of some trioctahedral micas with copper sulfate solutions at 25°C and 1 atmosphere: An electron microscope and transmission electron microscopy investigation. *Econ. Geol.* **87**: 1813–1829.

Jiang, W.-T. 1993. Diagenesis and very low-grade metamorphism of pelitic rocks from the Gaspé Peninsula, Québec: Ph. D. thesis. University of Michigan, Ann Arbor, Michigan, 269 pp.

Jiang, W.-T., F. Nieto, and D. R. Peacor. 1992. Composition of diagenetic illite as defined by analytical electron microscope analyses. Implications for smectite-illite-muscovite transition. (abstr.). 29th IGC Meeting, Kyoto, Japan, 100 pp.

Kim, J.-W., D. R. Peacor, D. Tessier, and F. Elsass. 1995. A technique for maintaining texture and permanent expansion of smectite interlayers for TEM observations. *Clays & Clay Miner.* (in press).

Kisch, H. J. 1983. Mineralogy and petrology of burial diagenesis (burial metamorphism) and incipient metamorphism in clastic rocks. In *Diagenesis in Sediments and Sedimentary Rocks.* G. Larsen and G. V. Chilingar, eds. New York: Elsevier, 289–493.

Laird, J. 1988. Chlorites: Metamorphic petrology. In *Hydrous Phyllosilicates.* S. W. Bailey, ed. Mineralogical Society of America, Reviews in Mineralogy, **19**: 405–453.

Lee, J. H., D. R. Peacor, D. D. Lewis, and R. P. Wintsch. 1984. Chlorite-illite/muscovite interlayered and interstratified crystals: A TEM/STEM study. *Contrib. Mineral. Petrol.* **88**: 372–385.

Lee, J. H., J. H. Ahn, and D. R. Peacor. 1985. Textures in layer silicates: Progressive changes through diagenesis and low temperature metamorphism. *J. Sed. Petrol.* **55**: 532–540.

Lee, J. H., D. R. Peacor, D. D. Lewis, and R. P. Wintsch. 1986. Evidence for syntectonic crystallization for the mudstone to slate transition at Lehigh Gap, Pennsylvania, U.S.A. *J. Struct. Geol.* **8**: 767–780.

Livi, K. J. T., D. R. Veblen, and J. M. Ferry. 1988. Electron microscope study of anchizone and epizone metamorphosed shales from the central Swiss Alps. *Geol. Soc. Amer. Abstracts with Programs* **20**: A244.

Li, G., D. R. Peacor, R. J. Merriman, B. Roberts, and B. A.

van der Pluijm. 1994. TEM and AEM constraints on the origin and significance of chlorite-mica stacks in slates: An example from central Wales, U.K. *J. Struct. Geol.* **16**: 1139–1157.

Mauk, J. L. 1993. Geological and geochemical investigations of the White Pine sediment-hosted stratiform copper deposit, Ontonagon County, Michigan: Ph. D. thesis. University of Michigan, Ann Arbor, Michigan, 194 pp.

Mauk, J. L., and G. B. Hieshima. 1992. Organic matter and copper mineralization at White Pine, Michigan. *Chem. Geol.* **99**: 189–211.

Mauk, J. L., W. C. Kelly, and B. A. van der Pluijm. 1992. Relations between deformation and sediment-hosted copper mineralization: Evidence from the White Pine portion of the Midcontinent rift system. *Geology* **20**: 427–430.

Meinschein, W. G., E. S. Barghoorn, and J. W. Schopf. 1964. Biological remnants in a Precambrian sediment. *Science* **145**: 262–263.

Merriman, R. J., B. Roberts, and D. R. Peacor. 1990. A Transmission electron microscope study of white mica crystallite size distribution in the mudstone to slate transitional sequence, North Wales, UK. *Contrib. Mineral. Petrol.* **106**: 27–40.

Morad, S. 1986. Mica-chlorite intergrowths in very low-grade metamorphic sedimentary rocks from Norway. *Jeues Jahrb. Mineral. Abh.* **154**: 271–287.

Morad, S., and A. A. AlDahan. 1986. Diagenetic alteration of detrital biotite in Proterozoic sedimentary rocks from Sweden. *Sediment. Geol.* **47**: 95–107.

Nishioka, G. K. 1983. Origin of late veins in the White Pine copper deposits, northern Michigan: M.S. thesis. University of Michigan, Ann Arbor, Michigan, 35 pp.

Ohr, M. 1993. Geochronology of diagenesis and low-grade metamorphism in pelites: Ph.D. thesis. University of Michigan, Ann Arbor, Michigan, 147 pp.

Peacor, D. R. 1992. Diagenesis and low-grade metamorphism of shales and slates. In *Minerals and Reactions at the Atomic Scale: Transmission Electron Microscopy.* P. R. Buseck, ed. Mineralogical Society of America, Reviews in Mineralogy **27**: 335–380.

Perry, E., and J. Hower. 1970. Burial diagenesis in Gulf Coast pelitic sediments. *Clays & Clay Miner.* **18**: 165–177.

Price, K. L., and S. D. McDowell. 1993. Illite/smectite geothermometry of the Proterozoic Oronto Group, Midcontinent rift system. *Clays & Clay Miner.* **41**: 134–147.

Ramamohan Rao, T. 1977. Distribution of elements between coexisting phengite and chlorite from the greenschist facies of the Tennant Creek area, central Australia. *Lithos* **10**: 103–112.

Shau, Y.-H., D. R. Peacor, and J. E. Essene. 1990. Corrensite and mixed-layer chlorite/corrensite in metabasalt from

northern Taiwan: TEM/AEM, EMPA, XRD, and optical studies. *Contrib. Mineral. Petrol.* **105**: 123–142.

Sliney, R. E. 1988. Comparative mineralogy and geochemistry of a stratigraphic unit within the upper shale member of the Nonesuch Formation, White Pine, Michigan. Unpub. M.S. thesis. University of Michigan, Ann Arbor, 60 pp.

Środoń, J., D. J. Morgan, E. V. Eslinger, D. D. Eberl, and M. R. Karlinger. 1986. Chemistry of illite/smectite and end-member illite. *Clays & Clay Miner.* **34**: 368–378.

Thwaites, F. T. 1912. Sandstones of the Wisconsin coast of Lake Superior. *Wisconsin Geological and Natural History Survey Bulletin* **25**: 117 pp.

Veblen, D. R., and J. M. Ferry. 1983. A TEM study of the biotite-chlorite reaction and comparison with petrographical observation. *Amer. Mineral.* **68**: 1160–1168.

Velde, B. 1977. *Clays and Clay Minerals in Natural and Synthetic Systems.* Amsterdam: Elsevier, 218 pp.

Velde, B., J. F. Raoult, and M. Leikine. 1974. Metamorphosed berthierine pellets in Mid-Cretaceous rocks from northeastern Algeria. *J. Sed. Petrol.* **44**: 1275–1280.

Weaver, C. E. R. 1984. Shale-slate metamorphism in southern Appalachian. *Development in Petrology.* Amsterdam: Elsevier, 239 pp.

White, W. S. 1966. Tectonics of the Keweenawan Basin, western Lake Superior region. *U.S. Geol. Survey Prof. Paper* **524-E**: E1–23.

White, W. S. 1971. A paleohydrologic model for mineralization of the White Pine copper deposit, northern Michigan. *Econ. Geol.* **66**: 1–13.

White, W. S., and J. C. Wright. 1966. Sulfide mineral zoning in the basal Nonesuch Shale, northern Michigan. *Econ. Geol.* **61**: 1171–1190.

White, S. H., J. M. Huggett, and H. F. Shaw. 1985. Electron-optical studies of phyllosilicate intergrowths in sedimentary and metamorphic rocks. *Mineral Mag.* **49**: 413–423.

Wiese, Jr., R. G. 1973. Mineralogy and geochemistry of the Parting Shale, White Pine, Michigan. *Econ. Geol.* **68**: 317–331.

Yau, Y.-C., D. R. Peacor, and S. D. McDowell. 1987. Smectite to illite reaction in Salton Sea shales: A transmission and analytical electron microscopy study. *J. Sed. Petrol.* **57**: 335–342.

Yau, Y.-C., D. R. Peacor, E. B. Richard, E. J. Essene, and S. D. McDowell. 1988. Microstructures, formation mechanisms, and depth-zoning of phyllosilicates in geothermally altered shales, Salton Sea, California. *Clays & Clay Miner.* **36**: 1–10.